Soft Matter

Accepted Manuscript

ROYAL SOCIETY OF CHEMISTRY

www.rsc.org/softmatter

Soft Matter

ARTICLE

Stimuli-responsive cylindrical hydrogels mimic intestinal peristalsis to propel a solid object

arbReceived 00th January 20xx,
Accepted 00th January 20xx

DOI: 10.1039/x0xx00000x

www.rsc.org/

V. Nistor,[a]† J. Cannell,[a] J. Gregory[a] and L. Yeghiazarian[a]†

The emerging field of soft robotics relies on soft, stimuli-responsive materials to enable load transport, manipulation, and mobility in complex unconstrained environments. These materials often need to replicate biological functionality such as muscle contractions and flexibility. Here we demonstrate a soft manipulator prototype based on thermosensitive PNIPAAM hydrogels that can transport and manipulate objects. A hollow cylindrical hydrogel was selectively heated and cooled with Peltier devices to yield a traveling wave of shrinking and swelling akin to intestinal peristalsis. A 4mm diameter bead was placed inside the cylinder and propelled 19.5 mm, equal to distance traveled by the peristaltic wave. We derived conditions that enable peristaltic transport as a function of transporter-cargo design parameters. We conclude that hydrogel-based peristaltic manipulators covering 2 orders of magnitude in stiffness ($1 \div 10^2$kPa) could transport cargo spanning 4 orders of magnitude in size (μm÷m).

1. Introduction

Load manipulation and transport is a challenge that arises in many areas of engineering and covers a wide range of scales. The emerging field of soft tools and robotics in particular needs new mechanisms of load transport and manipulation that can work in complex unstructured environments. Such mechanisms often require replication of some biological functionalities like muscle contractions and mobility, as well as gentle interactions with objects or the surrounding environment [1-4]. For instance, most medical tools are made of hard materials but are employed in soft environments and handle soft tissues. This lack of compliance matching in mechanical properties of the contacting materials often leads to high interfacial stresses and increases the likelihood of injury to soft tissues. Soft tools would eliminate this concern. Similarly, soft, deformable devices perform better in explorations of complex geometries, whether as part of body cavity probing, or field rescue operations and disaster relief[5].

Development of such devices has been accompanied by efforts to generate suitable materials, with emphasis on soft and stimuli-sensitive, or "smart", materials [6-11]. Smart, soft materials form the basis of machines found commonly in nature, such as heart muscles or eye lenses, which stand in contrast to machines in engineering that use mostly hard materials. Stimuli-responsiveness coupled with softness enables a wide range of functionalities, such as deformation in response to touch, adjustment of the focal length of the eye, regulation of water flow in plants, *etc* [12-14]. Polymer-based hydrogels are at the forefront in the development of soft, smart materials due to their versatility and applicability in a wide range of engineering fields including biomedical, electrical and environmental engineering, micro- and nanoengineering, robotics and pharmaceutics[15-23]. Not only stimuli-responsive polymer hydrogels have been incorporated as functional components in many engineered devices, but also entire systems have been engineered exclusively from hydrogels[24-29].

Hydrogels have been synthesized to respond to changes in varied environmental factors, such as temperature, electric field, pH, and radiation forces, whereby response often takes form of shape transformation such as deformation, or dramatic change in volume [22, 26, 30-33]. They can form the foundation of soft, deformable devices, because shape change can be utilized to transport and manipulate loads. For example, beads and cylinders can be transported over self-oscillating hydrogel "conveyer" sheets. In this case, the swelling-shrinking waves that propagate along the conveyer are driven by the Belousov-Zhabotinsky reaction, and oscillations are sustained until the reactants are consumed[34, 35]. The same principle has been used in tubular hydrogels to move liquids and resulting gas bubbles[3]. In our earlier work, we took advantage of propagating volume phase transitions to transport a bead attached to the tip of a cylindrical temperature-sensitive poly-N-isopropyl-acrylamide (PNIPAM) gel[33, 36]. In that case, the gel was synthesized in a glass tube, and the swelling/shrinking wave was induced using a series of Peltier elements to sequentially heat and cool segments of the gel. As opposed to self-oscillating gels, this set up allows for external control of the shape changes along the body of the gel; and the experiment could be repeated multiple times with the same gel.

[a] *Department of Biomedical Chemical and Environmental Engineering, University of Cincinnati, USA*
† *Corresponding authors: licaseverin@gmail.com, yeghialt@ucmail.uc.edu,*

Here we build upon this work to demonstrate a first peristaltic actuator to transport a solid object within a hollow cylindrical hydrogel by simulating the peristaltic motion of an intestine. The solid object is a bead inserted into the inner channel of the hydrogel (Figure 1). The shape of the hydrogel, and by extension the resulting contracting wave, is controlled with Peltier elements. As the hydrogel was heated from the left, the cylindrical walls contracted inwards thus reducing the available space in the channel and gently pushing the bead to the right. This prototype lays the foundation for explorations in soft delivery systems in medicine, whereby both the load and the surrounding soft tissues would be protected from injuries. Another area of study arising from this work is in soft, stimuli-responsive prosthetics and tissue supplements/replacements.

2. Results and Discussion

2.1 Hydrogel actuator assembly and control mechanism

A hollow cylindrical Laponite-PNIPAM hydrogel was synthesized inside a glass tube (see Experimental Methods). These particular hydrogels were selected due to their mechanical stability and relatively fast kinetics[32, 37]. Peltier elements were mounted along the glass tube using heat-conducting paste to deliver localized heating and cooling to the gel. A small segment of the hydrogel close to its left edge was dyed yellow to serve as a reference point. A 159 mg PMMA (poly (methyl methacrylate)) bead of 4 mm in diameter was initially positioned in the inner channel of the hydrogel such that the center of the bead was in line with the second pair of Peltier devices 2 and 8 (Figures 1, 2a).

Power was first supplied to the leftmost pair of Peltier elements 1 and 7 to create localized heating to the glass tube (Figure 2a). This induced a localized volume phase transition in the hydrogel that constricted the inner channel to the left of the bead. As the gel contracted inwards, it imparted a lateral force on the left side of the bead and pushed it through the channel to the right. Once the hydrogel phase transition pushed the bead past the adjacent pair of Peltier elements 2 and 8, the power to elements 1 and 7 was turned off (Figure 2b). Power to elements 2 and 8 was turned on and gradually increased to continue the wave of thermally induced phase transition that contracted the gel. After the bead had traveled past the third pair of Peltier devices 3 and 9, the power to elements 2 and 8 was turned off. Similar steps were taken to turn power on and off to the Peltier pair 3 and 9 (Figure 2c), and ultimately the Peltier pair 4-10 (Figure 2d), until the bead reached the end of the hydrogel channel. At this point all Peltier devices were turned off, the hydrogel was allowed to rehydrate (Figure 2e), and distance traveled by the bead was measured relative to the quad ruled paper visible at top of Figure 1a. This process, in essence, imitated the travelling peristaltic wave in the human small intestine, where smooth muscle contraction forces a bolus of food to travel down the intestine. The intestinal wall muscles then relax, and the intestine assumes its normal size.

2.2 Peristaltic transport

At the end of the experiment, the spherical bead was transported a total distance of 19.5 mm, equal to the distance travelled by the controlled heat wave as measured between the centerline of Peltier elements 1 and 4 (Figure 3). The travel of the bead was due solely to peristalsis; the experimental setup was designed to control for other possible transport mechanisms by using a hydrogel of length equal to the length of glass tube, and by sealing both ends of the tube.

Successful peristaltic transport relies on the bead staying in front of the contraction wave. In this experiment, localized control of phase change is achieved through careful balancing of the amount of heat transferred into the hydrogel from Peltier elements, against the amount of heat lost in the aqueous environment. Phase change in the Laponite-PNIPAM hydrogel occurs at the lower critical solution temperature (LCST) of 33°C. By controlling the magnitude of the electrical current delivered to each pair of Peltier devices, localized heating of the hydrogel is maintained just above the LCST behind the bead, and just below the LCST in front of the bead. Increasing heat output from the Peltier elements could bring the hydrogel in front of the bead to above the LCST as well, thus restricting the channel and effectively clamping the bead.

Heating of the Peltier elements makes the thermally conductive paste flow at the interface with the glass tube. This results in misalignment in Peltier pairs (e.g. 1 and 7) relative to the cross-sectional plane of the tube.

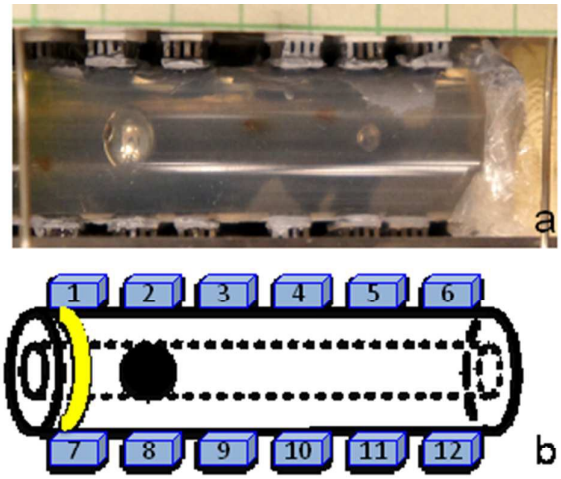

Figure 1. The experimental setup. The top image shows a hollow cylindrical Laponite-PNIPAM gel within a glass tube. The bead is inserted in the inner channel of the gel. The yellow band on the left side of the gel serves as a reference. The Peltier elements are pressed against the glass tube. Quad ruled paper is positioned in the background with each square being 5x5 mm. The schematic below mirrors the experimental setup and shows numbers assigned to each Peltier device.

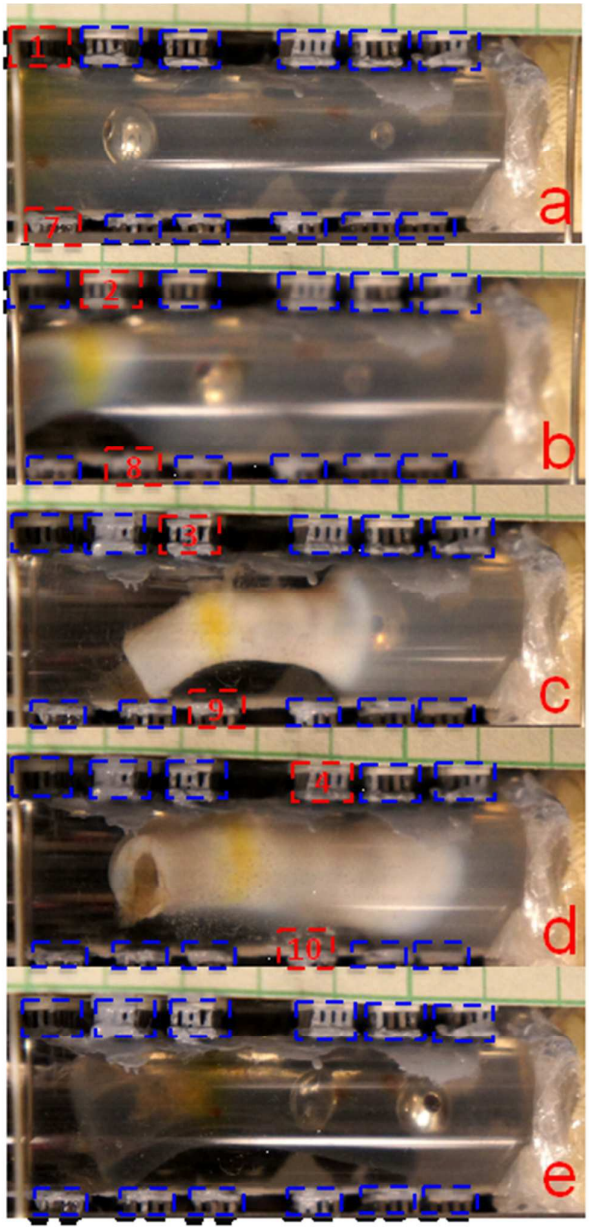

Figure 2. Peristaltic transport mechanism. Powered Peltier elements are shown in red, and unpowered elements in blue. Powered Peltier devices to the left of the bead induce a volume phase transition in the gel. As the volume phase transition is propagated from left to right by controlling the power to the Peltier devices, the gel contracts inward and gently pushes the bead to the right. An air bubble can be seen in the channel as well. Each square of quad ruled paper in the background is 5x5 mm.

Due to this asymmetry, the shrinking gel, as well as the contractile wave in its inner channel, were also asymmetrical. As a result, this contractile wave not only pushed the bead forward, but also imparted some rotation around its center point, as seen by observing the position of the hole in the center of the bead (Figures 2, 3). This suggests that controlling the shape and symmetry of the shrinking and swelling wave could provide a measure of dexterity to hydrogel-based actuators and manipulators. In addition to longitudinal transport, peristalsis can thus be used to impart additional cargo handling capabilities such as orientation control, opening new opportunities in development of soft manipulators and actuators for biomedical applications.

Another relevant feature of the control system design implemented in this study is that the gel can be controlled in real time, and necessary adjustments can be made to manipulate the cargo during transport. This is unlike the gels driven by the Belousov-Zhabotinsky (BZ) reaction, which oscillate autonomously until all reactants are consumed.

2.3 Design parameters for peristaltic actuator

2.3.1 Analysis of contact zone between actuator and load

Figure 4a shows a cross-section into the hydrogel tube that highlights how the shrinking gel envelops the bead along a spherical zone contact patch $A_1A_2A_3A_4$. Height p of spherical zone of contact between the bead and the gel has two separate components, as seen in Figure 4b, $p=p_1+p_2$. Reduction of cylinder diameter during shrinking causes the gel to wrap around the bead with a peristaltic wave of height p_1, whereas p_2 results from the bead indentation into the collapsed gel. In general, based on the Hertz contact theory, the contact half-width p_2 is a function of: (1) the reduced curvature R of interface between the spherical load and the hydrogel actuator, (2) the reduced Young's modulus E of the two materials, (3) the contact length $L=2\pi R_1$ (Figure 4a), and (4) the

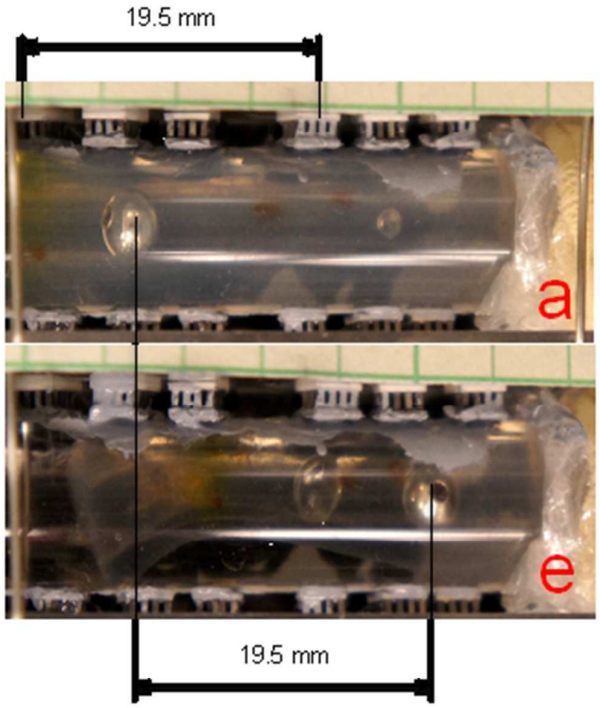

Figure 3. Measurement of peristaltic transport of the bead in the inner channel of the gel based on bead position at the start Figure 2a and finish Figure 2e.

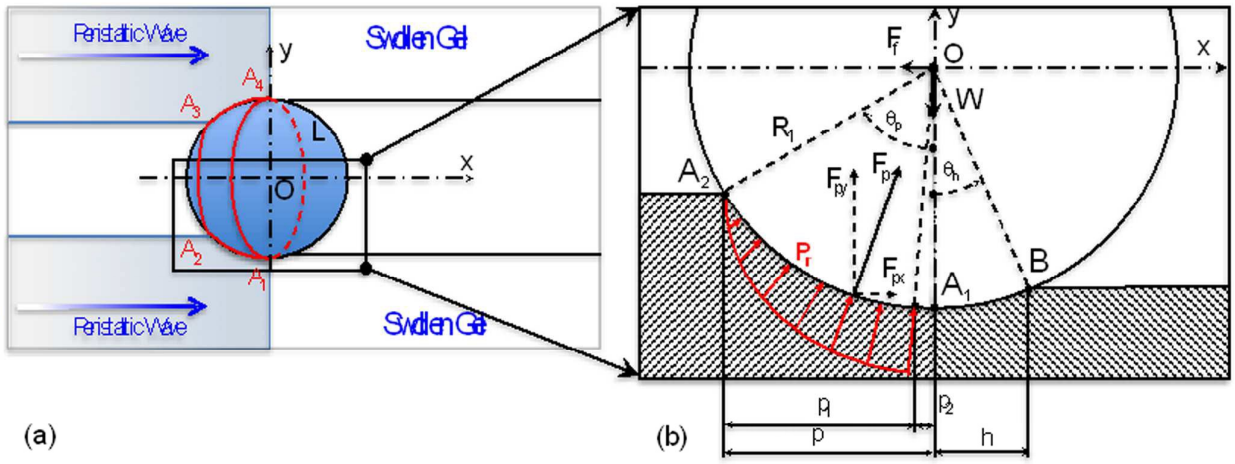

Figure 4. (a) Cross-sectional schematic of peristaltic transport of a spherical bead in the inner channel of the cylindrical hydrogel along the longitudinal x-axis. The contact patch between the peristaltic wave and the bead is the spherical zone (shown in red $A_1A_2A_3A_4$) of surface $S_p=2\pi R_1 p_1$. **(b)** Balance of forces acting on the bead. F_p is the peristaltic force, resulting from the pressure P_r *(shown in red)* exercised by the peristaltic wave on the spherical zone $A_1A_2A_3A_4$. F_h is the force resulting from contact between bead and hydrated gel on the spherical zone surface $S_h=2\pi R_1 h$. W is the load (weight minus buoyancy) of the bead in the aqueous environment. Indentation caused by bead on the dehydrated gel is p_2.

effective load W [34]:

$$p_2 = \sqrt{\frac{8RW}{\pi EL}} \qquad (1)$$

The reduced curvature R is calculated from

$$\frac{1}{R} = \frac{1}{R_1} + \frac{1}{R_{gel}} \qquad (2)$$

where R_1 is the radius of the bead, and R_{gel} is the curvature radius of the hydrogel actuator. The collapsed section of the gel wraps around the bead and therefore its radius is equivalent to the radius of the bead, $R_{gel} = R_1$, making the reduced curvature of the collapsed section $R = ½R_1$. The swollen section of the gel however is a linear actuator and its radius is therefore $R_{gel} = \infty$. Therefore, the reduced curvature of the swollen section is $R = R_1$.

The reduced Young's modulus E is

$$E = \frac{2}{\left[\frac{1-\nu_{bead}^2}{E_{bead}} + \frac{1-\nu_{gel}^2}{E_{gel}}\right]} \qquad (3)$$

where ν_{bead} and ν_{gel} are respective Poisson ratios (Table 1). Since the PMMA bead is much stiffer than the hydrogel (E_{bead} ~10^9 Pa vs E_{gel} ~10^3 Pa), the reduced Young's modulus can be approximated as

$$E = \frac{2E_{gel}}{1-\nu_{gel}^2} \qquad (4)$$

Voudouris *et al* have shown that following a volumetric phase transition PNIPAM hydrogels maintain the same Poisson ratio ν_{gel} =0.4, but the elastic modulus is about 7-8 times larger for the collapsed gel[38]. Therefore, according to Eq. (4), the reduced Young's modulus for the swollen and the collapsed sections of the gel maintains the same ratio.

The effective load is

$$W = {}^4/_3 \pi R_1^3 g(\rho_{bead} - \rho_{water}) \qquad (5)$$

where ρ_{bead} and ρ_{water} are the density of the bead and of water, respectively. Materials properties for the hydrogel actuator and the bead used in this study are summarized in Table 1.

Taking these substitutions back into Eq. (1) and using respective parameter values for collapsed gels, yields a contact half width for the collapsed gel $p_2 \approx ¼h$, where h is the contact half width for the swollen section of the gel. Considering that the collapsed gel wraps around the bead, further distributing its load W along the arc of the peristaltic wave, the contact half width p_2 is further diminished to the point of being negligible compared to h, *and* $p_1 \approx p$ as depicted in Figure 4b. We conclude therefore that the shape of the peristaltic wave in contact with the load is driven primarily by narrowing of the inner diameter of the gel cylinder during phase transition, and to a much lesser extent due to indentation in the gel caused by the load.

2.3.2. Balance of forces and conditions for peristaltic transport

The shrinking hydrogel applies radial pressure P_r on the bead, which derives from the hoop stress σ_h in the cylindrical wall (Figure 4b). For thin walls, the pressure on the bead depends on the cylinder's mean radius *r*, and its wall thickness *t*:

$$P_r = \frac{\sigma_h t}{r} \quad (6)$$

where mean radius *r* is computed as

$$r = \frac{r_{out} + r_{in}}{2} \quad (7)$$

where r_{out} and r_{in} are the outer and inner radii of the cylinder. In our experiment, the maximum value of P_r occurs at the point A_1, and the minimum (zero) value occurs at point A_2 (Figure 4b). At point A_1,

$$r_{out} = R_1 + t \text{ and } r_{in} = R_1 \quad (8)$$

Therefore, at point A_1, $t=R_1$ and

$$P_{r\,max} = \frac{2}{3}\sigma_h \quad (9)$$

Hoop stress in the wall of the cylinder is equivalent to the normal compressive and elongation stress in a flat sample. Illeperuma *et al* measured the force developed by a flat swelling PNIPAM hydrogel constrained between parallel plates[39]. After 24 hours, a 10 mm diameter and 5mm thickness hydrogel sample yields a force of about 0.65N along its longitudinal axis. Compressive stress in the hydrogel sample, calculated as force divided by the cross-sectional area of the sample, equals 8.3kPa. It is reasonable to assume that reversing from hydrogel swelling to contraction would yield a similar elongation stress. For a flat gel rolled into a cylinder with free ends, the elongation stress yields the cylinder hoop stress along the section where the bead is in contact with the shrinking gel. Maximum hoop stress $\sigma_{h\,max}=8.3kPa$ occurs at A_1 and varies linearly around arc A_1A_2, such that at A_2, $\sigma_h=0$.

The resulting radial pressure P_r is therefore also linearly distributed along the arc of contact A_1A_2, as shown in Figure 4b. Since the maximum pressure $P_{r\,max} = 2/3\ \sigma_{h\,max}$ occurs at A_1 and no pressure at A_2, we approximate that the average pressure $P_{r\,avg} = ½\ P_{r\,max} = 1/3\ \sigma_{h\,max}$ is evenly distributed over the arc of contact A_1A_2. The peristaltic wave therefore acts on the spherical zone of surface $S_p = 2\pi R_1 p$ with force

$$F_p = P_{r\,avg} S_p = \frac{2}{3}\sigma_{h\,max}\pi R_1 p \quad (10)$$

where R_1 is the radius of the bead, and $p=R_1 sin\theta_p$ is the height of the spherical zone. Eq. (10) then simplifies to

$$F_p = \frac{2}{3}\sigma_{h\,max}\pi R_1^2 \sin\theta_p \quad (11)$$

The point of application for F_p is in the centre of mass for the pressure distribution, 1/3rd of the arc A_1A_2 away from A_1. To initiate peristaltic propulsion, the horizontal *Ox* projection F_{px} of the force generated by the peristaltic wave F_p has to overcome the friction force F_f between the bead and the swollen gel:

$$F_{px} > F_f \quad (12)$$

where

$$F_{px} = F_p \sin\left(\frac{\theta_p}{3}\right) \quad (13)$$

Friction force is

$$F_f = \mu W \quad (14)$$

where μ is the friction coefficient. Eq. (12) can be rewritten as

$$\frac{2}{3}\sigma_{h\,max}\pi R_1^2 \sin\theta_p \sin\frac{\theta_p}{3} > \frac{4}{3}\mu\pi R_1^3 g(\rho_{bead} - \rho_{water}) \quad (15)$$

After reduction of like terms and a Taylor series expansion of the trigonometric terms, Eq. (15) becomes

$$\theta_p > \sqrt{6\frac{\mu}{\sigma_{h\,max}} R_1 g(\rho_{bead} - \rho_{water})} \quad (16)$$

Eq. (16) is the condition for which peristaltic transport is possible. It relates the minimum value of the peristaltic wave angle θ_p to physical parameters of the actuator, the cargo and friction. The maximum value of θ_p can be calculated from geometry shown in Figure 4b. For PNIPAM hydrogel used in our study, the ratio between the swollen and collapsed radii of the cylinder is approximately two [38], therefore $\theta_{p\,max} \approx 60°$.

Table 1. Material properties

Parameters	Notation	Values
Hydrogel Actuator		
Swollen gel		
Curvature Radius	R_{gel}	∞
Young's Modulus	E_{gel}	*2.16 x 10³ Pa*
Poisson ratio	v_{gel}	*0.4*
Collapsed gel		
Curvature Radius	R_{gel}	R_1
Young's Modulus	E_{gel}	*8 x 2.16 x 10³ Pa*
Poisson ratio	v_{gel}	*0.4*
Spherical bead		
Radius	R_1	*2 mm*
Young's Modulus	E_{bead}	*3.00 x 10⁹ Pa*
Poisson ratio	v_{bead}	*0.33*
Density	ρ_{bead}	*1.19 g/cm³*
Water density	ρ_{water}	*1.00 g/cm³*

2.3.3. Friction

One the most relevant parameters to peristaltic transport is the sliding friction between the bead and the swollen gel. Yashima *et al* investigated the sliding of PNIPAM hydrogels on glass surface in aqueous environment and found the critical measure to be the normal pressure at which the lubricating water film breaks down[40]. For normal pressure less than 500Pa, the thickness of the lubricating water film is over *100 ÷ 150 μm*, corresponding to a very small friction coefficient $\mu = 0.016 \div 0.020$. As the normal pressure increases over the 500Pa, the lubricating water film quickly collapses to less than *10 ÷ 20 μm thickness,* and the friction coefficient increases rapidly to $\mu > 0.5$ [40, 41]. As shown in Figure 5a, scaling both the actuator and the bead with R_1 in the range from 1*μm* to 1m, the normal pressure between the load and the PNIPAM hydrogel reaches 500Pa as the radius of the bead increases over the R_1>100mm. The maximum force $F_{px\ max}$ that the PNIPAM hydrogel can produce when fully collapsed, corresponds to the $\theta_{p\ max} = 60°$. For R_1<100mm, Figure 5b shows that the friction force F_f is orders of magnitude smaller than the $F_{px\ max}$. However over 100mm bead radius, the friction force quickly approaches and overcomes F_{px}, to the point of stopping the peristaltic transport. Therefore, controlling θ_p from the minimum value required to produce peristaltic transport to a maximum of 60° shows that cargo-handling capabilities of scaled PNIPAM-Laponite hydrogels could cover up to four orders of magnitude from micrometer up to meter-sized cargo (Figure 5b).

It is also possible to vary the elastic modulus of the swollen gel. For the cargo used for this experiment (R_1=2mm and E_{bead}~3GPa), peristaltic transport mechanism can be achieved using a variety of PNIPAM hydrogel formulations with stiffness covering a wide spectrum of Young's moduli from 1 to 150 KPa (Figure 5c)[42]. The combination of small-size cargo and stiffer hydrogels has the potential to enable peristaltic transport at small θ_p, and therefore be more conducive to faster transport by requiring a smaller swelling/shrinking volume ratio. Promising new PNIPAM hydrogel developments are much stiffer, *e.g.* E_{gel}~10÷50 KPa[42], and therefore should require a value of θ_p less than one degree to initiate peristaltic transport for mm-sized cargo. However the combination of increased cargo size and higher stiffness hydrogels would run into the limitations associated with water film as lubricant. Friction modifying strategies [43-45] would need to be employed such that the friction coefficient stays small even as the normal pressure between bead and hydrogel reaches into the kPa range, see Figure 5c.

The design of the system control can also be optimized for more efficient transport. The maximum stroke of the peristaltic actuator is measured as the hydrogel is fully collapsed behind the bead to its minimum diameter, ½ its original inner diameter. That makes the stroke equal to $R_1 sin\theta_{p\ max}$. This suggests that optimal separation between the heating sources (Peltier elements) should be smaller than the maximum stroke.

4. Experimental Methods

Laponite-PNIPAM hydrogels were synthesized as in [32]. A hollow glass cylinder of 100 mm in length and inner diameter of 10 mm was cut from borosilicate tubing. A solid glass rod of 5.1 mm in diameter was suspended concentrically within the glass cylinder. Both were silanized for hydrophobicity by submerging the glass in a solution of distilled water, acetic acid (1.0% wt, Sigma-Aldrich) and diethoxydimethylsilane (5.0% wt., Sigma-Aldrich) then dried for 20 minutes in a vacuum oven at 113°C [33]. Pre-gel solution was injected into the void and polymerized for 24 h. The rod was removed and hydrogel pulled from the cylinder with micro-forceps. The gel was submerged in DI water and fully swollen, followed by five complete cycles of shrinking and swelling to remove any residue. DI water was changed between each cycle. A 2 mm-wide segment of the gel surface at about 18 mm from the left end of the gel was dyed with acriflavine (Sigma Aldrich) to serve as a reference. The gel was placed back into the glass cylinder in which it was polymerized. A PMMA bead of 4 mm diameter was inserted in the channel in the center of the gel, and ends of the tube were sealed with polyethylene sheets.

Peltier elements (3.5mm x 5mm, Digi-Key) were fixed in two rows of 6 elements each along the glass cylinder on opposing sides (Figure 1). Thermal grease (Zalman Tech Co) was applied between the glass cylinder and Peltiers. Peltier were wired in parallel and connected to a variable power source (Tekpower, HY1803D), allowing heating or cooling to be selectively applied to the cylinder through any combination of elements.

Conclusions

In conclusion, we presented, for the first time, peristaltic

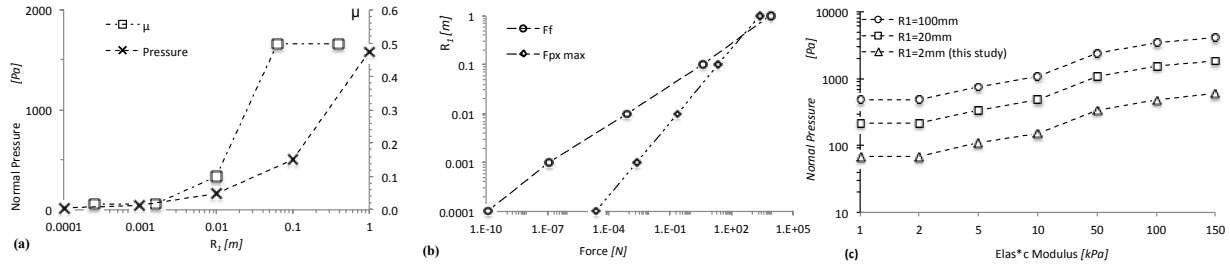

Figure 5. Estimated Design Parameters for the Peristaltic Transport Mode. (a) Scaling both the actuator and the bead with R_1 in the range from 1*μm* to 1m, the normal pressure between the load and the PNIPAM hydrogel reaches 500Pa as the radius of the bead increases over the R_1>100mm. At this point the friction coefficient increases drastically from $\mu < 0.02$ to $\mu > 0.5$. **(b)** As a result friction force F_f increases to the point peristalsis is no longer efficient for this PNIPAM formulation. **(c)** For this particular cargo R_1=2mm, PNIPAM hydrogels with a range of stiffness (E_{gel} = 1÷150 KPa) would produce peristaltic transport. Combinations of stiffer hydrogels and larger cargo need to employ friction modifying strategies for normal pressure above *500Pa*.

transport of a solid object within a soft, hollow cylindrical hydrogel, and derived conditions that enable peristaltic transport as a function of transporter-cargo design parameters. This experiment demonstrates a new mode of engagement of environmentally sensitive hydrogels as soft devices interfacing with and manipulating solid, hard objects. It is significant as it is likely to open new avenues for hydrogels in actuation, soft robotics and medical devices. Future studies should focus on optimization of gel kinetics to the specific application, as well as remote control of gel shape changes to allow for deployment in environments that are otherwise difficult to access.

Acknowledgements

This work was supported by the NSF CBET-1248385 grant, and the BCEE Seed Grant.

References

1. F. Iida and C. Laschi, *Proceedings of the 2nd European Future Technologies Conference and Exhibition 2011 (Fet 11)*, 2011, **7**, 99-102.
2. C. Lekakou, Y. Elsayed, T. Geng and C. M. Saaj, *Advanced Engineering Materials*, 2015, **17**, 1180-1188.
3. Y. Shiraki and R. Yoshida, *Angew. Chem.-Int. Edit.*, 2012, **51**, 6112-6116.
4. F. Ilievski, A. D. Mazzeo, R. E. Shepherd, X. Chen and G. M. Whitesides, *Angew. Chem.-Int. Edit.*, 2011, **50**, 1890-1895.
5. C. Majidi, *Soft Robotics*, 2014, **1**, 5-11.
6. Y. Samchenko, Z. Ulberg and O. Korotych, *Adv. Colloid Interface Sci.*, 2011, **168**, 247-262.
7. M. A. C. Stuart, W. T. S. Huck, J. Genzer, M. Muller, C. Ober, M. Stamm, G. B. Sukhorukov, I. Szleifer, V. V. Tsukruk, M. Urban, F. Winnik, S. Zauscher, I. Luzinov and S. Minko, *Nat. Mater.*, 2010, **9**, 101-113.
8. I. Tokarev and S. Minko, *Soft Matter*, 2009, **5**, 511-524.
9. R. Yoshida, *Curr. Org. Chem.*, 2005, **9**, 1617-1641.
10. G. J. Dunderdale and J. P. A. Fairclough, *Langmuir*, 2013, **29**, 3628-3635.
11. Z. L. Wu, M. Moshe, J. Greener, H. Therien-Aubin, Z. H. Nie, E. Sharon and E. Kumacheva, *Nature Communications*, 2013, **4**.
12. Z. Suo, *Mrs Bulletin*, 2012, **37**, 218-225.
13. Y. Moriyama, S. Hiyama and H. Asai, *Biophysical Journal*, 1998, **74**, 487-491.
14. Y. Moriyama, H. Okamoto and H. Asai, *Biophysical Journal*, 1999, **76**, 993-1000.
15. S. Coradeschi, H. Ishiguro, M. Asada, S. C. Shapiro, M. Thielscher, C. Breazeal, M. J. Mataric and H. Ishida, *Ieee Intelligent Systems*, 2006, **21**, 74-85.
16. J. J. Kang Derwent and W. F. Mieler, *Transactions of the American Ophthalmological Society*, 2008, **106**, 206-213; discussion 213-204.
17. N. Kashyap, N. Kumar and M. Kumar, *Crit. Rev. Ther. Drug Carr. Syst.*, 2005, **22**, 107-149.
18. T. Miyata, M. Jige, T. Nakaminami and T. Uragami, *Proc. Natl. Acad. Sci. U. S. A.*, 2006, **103**, 1190-1193.
19. M. Sirousazar, M. Kokabi and Z. M. Hassan, *J. Appl. Polym. Sci.*, 2012, **123**, 50-58.
20. D. Svirskis, J. Travas-Sejdic, A. Rodgers and S. Garg, *J. Control. Release*, 2010, **146**, 6-15.
21. A. K. Agarwal, S. S. Sridharamurthy, D. J. Beebe and H. R. Jiang, *Journal of Microelectromechanical Systems*, 2005, **14**, 1409-1421.
22. R. H. Liu, Q. Yu and D. J. Beebe, *Journal of microelectromechanical systems*, 2002, **11**, 45-53.
23. G. H. Kwon, J. Y. Park, J. Y. Kim, M. L. Frisk, D. J. Beebe and S. H. Lee, *Small*, 2008, **4**, 2148-2153.
24. P. Dayal, O. Kuksenok and A. C. Balazs, *Langmuir*, 2009, **25**, 4298-4301.
25. O. Kuksenok, V. V. Yashin, P. Dayal and A. C. Balazs, *J. Polym. Sci. Pt. B-Polym. Phys.*, 2010, **48**, 2533-2541.
26. S. Maeda, Y. Hara, T. Sakai, R. Yoshida and S. Hashimoto, *Adv. Mater.*, 2007, **19**, 3480-+.

27. S. Maeda, Y. Hara, R. Yoshida and S. Hashimoto, *Angew. Chem.-Int. Edit.*, 2008, **47**, 6690-6693.
28. S. Maeda, Y. Hara, R. Yoshida and S. Hashimoto, *Macromol. Rapid Commun.*, 2008, **29**, 401-405.
29. J. Gregory, S. Riasi, J. Cannell, H. Arora, L. Yeghiazarian and V. Nistor, *J. Appl. Polym. Sci.*, 2014, **40927**.
30. S. Juodkazis, N. Mukai, R. Wakaki, A. Yamaguchi, S. MAtsuo and H. Misawa, *Nature*, 2000, **408**, 178-181.
31. L. Mahadevan, S. Daniel and M. K. Chaudhury, *Proc. Natl. Acad. Sci. U. S. A.*, 2004, **101**, 23-26.
32. H. Arora, R. Malik, L. Yeghiazarian, C. Cohen and U. Wiesner, *Journal of Polymer Science Part a-Polymer Chemistry*, 2009, **47**, 5027-5033.
33. L. Yeghiazarian, S. Mahajan, C. D. Montemagno, C. Cohen and U. B. Wiesner, *Adv. Mater.*, 2005, **17**, 1869-1873.
34. Y. Murase, M. Hidaka and R. Yoshida, *Sens. Actuator B-Chem.*, 2010, **149**, 272-283.
35. Y. Murase, S. Maeda, S. Hashimoto and R. Yoshida, *Langmuir*, 2009, **25**, 483-489.
36. L. Yeghiazarian, H. Arora, V. Nistor, C. D. Montemagno and U. Wiesner, *Soft Matter*, 2007, **3**, 939-944.
37. K. Haraguchi, H. J. Li, K. Matsuda, T. Takehisa and E. Elliott, *Macromolecules*, 2005, **38**, 3482-3490.
38. P. Voudouris, D. Florea, P. van der Schoot and H. M. Wyss, *Soft Matter*, 2013, **9**, 7158-7166.
39. W. R. K. Illeperuma, J.-Y. Sun, Z. Suo and J. J. Vlassak, *Soft Matter*, 2013, **9**, 8504-8511.
40. S. Yashima, N. Takase, T. Kurokawa and J. P. Gong, *Soft Matter*, 2014, **10**, 3192-3199.
41. A. C. Dunn, J. M. Uruena, Y. Huo, S. S. Perry, T. E. Angelini and W. G. Sawyer, *Tribology Letters*, 2013, **49**, 371-378.
42. L.-W. Xia, R. Xie, X.-J. Ju, W. Wang, Q. Chen and L.-Y. Chu, *Nature Communications*, 2013, **4**.
43. S. Ma, M. Scaraggi, D. Wang, X. Wang, Y. Liang, W. Liu, D. Dini and F. Zhou, *Adv. Funct. Mater.*, 2015, **25**, 7366-7374.
44. J. P. Gong, T. Kurokawa, T. Narita, G. Kagata, Y. Osada, G. Nishimura and M. Kinjo, *Journal of the American Chemical Society*, 2001, **123**, 5582-5583.
45. M. M. Blum and T. C. Ovaert, *Wear*, 2013, **301**, 201-209.